Contribution to the study of thunderstorms in the Congo Basin: Analysis of periods with intense activity

Jean Kasereka Kigotsi, Serge Soula, Albert Bantu Mukenga Kazadi, André Ndotoni Zana

Contribution to the study of thunderstorms in the Congo Basin: Analysis of periods with intense activity

Jean Kigotsi Kasereka[1], Serge Soula[2], Albert Kazadi Mukenga Bantu[1], André Zana Ndotoni[1].

[1]Département de Physique, Faculté des Sciences, Université de Kinshasa, Kinshasa, République Démocratique du Congo

[2]Laboratoire d'Aérologie, Université de Toulouse, UT3, CNRS, IRD, Toulouse, France

Abstract. Lightning activity, storm structures, meteorological and environmental conditions are analyzed within a large area of Central Africa (25° × 25°) for two periods of one month (March and December) with high thunderstorm activity in 2013. The lightning flashes issued from World-Wide Lightning Location Network (WWLLN) allow to contribute in highlighting some characteristics in agreement with the literature. Some new findings, that can be useful for future storm monitoring thanks to lightning data issued from ~~geostationary sensors as~~ the Lightning Imager (LI) onboard Meteosat Third Generation (MTG), have been noted and have to be confirmed with more case studies. Thus, a seasonal correlation is found between the daily flash number and the extent of large CAPE values. The lightning flash density exhibits the same location of its maximum, for December and March with about 3 and 2 flashes km^{-2}, respectively. This location is also reported in the literature for the annual activity in the study area. The storm developments often occur in the regions that combine the presence of lakes and mountains. The flash clusters allow to localize the strong convective activity and to follow the displacement of the storm systems when they move. The flash rate density (FRD) is larger in the convective systems well organized, as the typical MCS, during the development of the storms and when several cells merge. The daily cycle shows a lightning flash rate maximum between 14:00 and 15:00 UT that precedes the maximum development of the storm by one hour. It also shows that the storms that occur within the region of the main maximum of lightning activity, are more frequent and produce larger values of FRD.

1. Introduction

Global studies have shown that the world record for lightning at regional scale is observed in the Congo Basin (Christian et al., 2003; Cecil et al., 2014; Albrecht et al., 2011, 2016). The results

of those studies generated interest and motivated other works conducted within this region and around, to well understand the development of this activity. Thus, a detailed climatology of lightning activity at high resolution was elaborated for this region of Central Africa (Soula et al., 2016). This climatology especially highlighted two areas of strong lightning density. A subsequent work was conducted to compare the two areas describing them in more detail (Kigotsi et al., 2018). However, in the perspective of future spatial data regarding lightning activity and meteorology that will be especially provided by the geostationary satellite Meteosat Third Generation (MTG), the relationship between lightning and convective activities in Central Africa needs to be better studied (Stuhlmann et al., 2005).

According to the usual concept, strong lightning activity is a signature of convective intensity (Zipser et al., 2006). It is confirmed for the region of Congo Basin because the most intense thunderstorms around the world are found in equatorial Africa (Zipser et al., 2006). High lightning activity requires a microphysical environment of mixed phase and strong updrafts (Toracinta and Zipser, 2001). It is therefore natural that deep convection frequently exceeds the tropopause in the Congo Basin (Liu and Zipser, 2005). One of the causes of intense thunderstorms is the strong convective instability which initiates and maintains the ascents of humid air. The solar radiation, particularly high in the tropical region, is the source of energy necessary for strong updrafts which can generate thunderstorms when the CAPE is large. Indeed, it has been established that the diurnal convection cycle in the tropics is linked to the destabilization of the atmospheric boundary layer by solar radiance in the afternoon (Wallace, 1975; Dai et al., 1999; Dai, 2001). Observations have shown that the minimum of cloud top temperature (CTT) is associated with the maximum of lightning flash rate at scale of the thundercell (i.e. Williams et al., 1989; Soula et al., 2014). Indeed, the decrease in CTT directly reflects the vertical extension of the thunderstorm on the one hand, and the increase of lightning rate expresses charging/discharging processes within the thunderstorm on the other hand. So, there is a relationship between the lightning activity and the strong vertical development of thunderstorm systems. Strong updrafts that raise cloudy air masses to high altitude also promote hydrometeor collisions and consequently cloud electrification and lightning production (Takahashi, 1978; Saunders et al., 1991). But the vertical extension of thunderstorms is not the only phenomenon associated with the increase of lightning flash rate, that is also associated with other phenomena that affect thunderstorm cells, as merging, regeneration. These phenomena influence therefore also the level of lightning activity.

Mesoscale Convective Systems (MCSs) constitute the fundamental unit of vertical energy transport in Central Africa (Farnsworth et al., 2011). Deep convection is often organized in MCSs in that region. These systems have been found to be mainly generated on the western slopes of the Rift Valley mountains and then propagate westwards and southwestwards (Nguyen and Duvel, 2008; Laing et al., 2011). Singularly, orography certainly plays a role in the origin of the acute maximum of lightning density observed each year around 28°E and 2°S, in the Congo Basin. As the highest mountains exceeding 3000 meters altitude are located at about 28.5°E, their presence is a favorable element for the development of thunderstorms likely to produce a high density of lightning (Soula et al., 2016). It has also been found that convection in the region is not only initiated by the heating of upland areas but also by sea / land breeze and lake breeze (Laing et al., 2011). The local effect of sea or lake breezes as well as that of topography has also been observed in several other studies elsewhere in the world (Oki and Musiake, 1994; Yang and Slingo, 2001; Yang and Smith, 2006). Coherent episodes of convection have also been observed in this region as a result of convection regeneration through multiple diurnal cycles during westward propagation (Laing et al., 2011). Convection has also been shown to be modulated there by coupled Kelvin waves propagating eastward (Laing et al., 2011).

The zone defined by the range 5°S - 5°N in latitude and 10°E - 30°E in longitude practically coincides with the sector identified as the most active zone in terms of thunderstorm activity (Jackson et al., 2009). It extends approximately from the west coast of Africa on the Atlantic Ocean to the west of the Rift Valley. The main core of the maximum of MCSs number and the secondary core of the maximum of lightning flashes per MCS were found in the eastern part of this region (Jackson et al., 2009). On the same way, the main maximum of the lightning density in Soula et al. (2016) corresponds with the same location. In addition, a second core of MCS number and the main core of the maximum of lightning flashes per MCS were found in the central part of the region (Jackson et al., 2009), where Soula et al. (2016) found the secondary maximum of the lightning density. The maximum wind shear was also associated with the maximum of MCSs number in the central part. For example, during the March-May season and during the period 2000-2003, the peak of the wind shear at 925hPa was located at the same place as the secondary maximum of the lightning density (Jackson et al., 2009). Indeed, observations from other regions of tropical Africa have shown that deep convection is often associated with wind shear maxima in the 925-600 hPa layer of the troposphere (Laing et al., 2008; Mohr and Thorncroft, 2006). Another previous study

also highlighted the role of convergence in the lower layers of the troposphere in intense thunderstorm activity in central Africa. For example, it was reported the coincidence between the maximum of lightning density and the maximum of convergence in the middle troposphere (600 hPa) around 25°E - 30°E, in equatorial Africa, during the month of October over the period 1998 - 2003 (Jackson et al., 2009). In particular, it has also been shown that this convergence maximum coincides with a very marked maximum in the number of MCSs during the September-November season during which the AEJ-S jet, creator of this convergence, is well developed (Jackson et al., 2009).

In this paper we analyze the thunderstorm activity in this area of the Congo Basin during two periods of intense activity recorded in 2013. Based on results from Soula et al. (2016) for the climatology of lightning activity in the region of Congo Basin, we consider two months of 2013 (March and December) with a high flash number and a low variability to be representative of a strong activity as better as possible. Indeed, 2013 was the year with the best detection efficiency and these two months correspond with the best combination of a high flash number and a low variability out of the World-Wide Lightning Location Network (WWLLN) database available for the study. Figure 1 displays the study area (red frame) within the map of the African continent with the relief indicated with the colored scale. We analyze the temporal correlation between the CAPE and the number of lightning flashes at a resolution of the day on the whole area and for two months of activity. Then we examine the spatial correlation between the same parameters for two periods of 24 hours and finally we analyze the spatiotemporal correlation between the production of lightning and the cloud characteristics at several scales of time and space, according to the shape and the duration of convective systems. Thus, section 2 is devoted to the description of the data used and to the methodology, the section 3 to the presentation of the results at different time and space scales, section 4 to a discussion and finally section 5 to a summary of the main results.

2. Data and methodology

2.1 Lightning activity

Lightning activity is analysed from the data collected by the global lightning detection network World-Wide Lightning Location Network (WWLLN) that works around the Earth (www.wwlln.net/). As other ground Lightning Location Systems (LLS), it detects the electromagnetic radiation emitted by lightning strokes (from cloud-to-ground and intracloud

125 flashes) at very low frequency (VLF), called sferics (Abarca et al., 2011). The strokes location is
126 based on the time of group arrival technique (TOGA) technique (Dowden et al., 2002). Several
127 studies show that the WWLLN has been improved in terms of Detection Efficiency (DE) since its
128 implantation in March 2003. The increasing number of stations and the development of the
129 processing algorithm can explain this improvement (Rodger et al., 2008). To give an idea of the
130 growth of the number of WWLLN stations spread on the planet, it was 11 in 2003, then 23 in 2005,
131 30 in 2007 and 67 in 2013, according to the report made by Rodger et al. (2014). Indeed, the
132 changes in the network during the 10-year period (2003-2013) can explain the continuous increase
133 of the detection efficiency (DE) observed by Soula et al. (2016) in the same domain of the present
134 study. The average DE within the study area increased from 1.7 % in 2005 to 5.9 % in 2013, in
135 comparison to observation made by the Lightning Imaging Sensor (LIS) onboard TRMM, when it
136 was above the same thunderstorms (Soula et al., 2016). Actually, DE for CG flashes is about twice
137 that for IC flashes according to Abarca et al. (2011). It means the flashes we consider in the study
138 represent a sample of the total flash amount, which means the parameters derived from it (flash
139 rate, flash density) have to be considered as relative quantities. The flashes are reconstructed as in
140 Soula et al. (2016), i.e. successive strokes are associated within a flash when they are separated by
141 less than 0.5 s and less than 20 km. DE could change in the whole domain of study, with values up
142 to 7.5 % in 2013 for the 5° × 5° area of the main maximum activity (Kigotsi et al., 2018).
143
144 2.2 Cloud structure and meteorology
145 Cloud Top Temperatures (CTT) are provided by data from the Spinning Enhanced Visible
146 and Infrared Imager (SEVIRI) onboard the Meteosat Second Generation (MSG) satellite launched
147 and operated by the European Space Agency (ESA) and the European Organization for the
148 Exploitation of Meteorological Satellites (EUMETSAT), respectively. Thus, the radiometer
149 SEVIRI located at about 0° in latitude and longitude, scans the Earth disk to provide images in 12
150 spectral bands every 15 minutes at a spatial resolution of 0.027°, which corresponds to 3 km at
151 nadir, below the geostationary satellite. The thermal infrared band (IR) at ~11-13 μm allows to
152 estimate the CTT with an accuracy generally better than ~1°C. The parameters used in this study
153 derived from the CTT are the minimum of CTT for a given area noted min(CTT), the fractional
154 area noted as :
155 $$A(\tau), \text{ when } CTT < \tau$$

156 $A(\tau_1 ; \tau_2)$ when $\tau_1 < CTT < \tau_2$

157 The CTT allows to make maps ~~of CTT~~ each 15 minutes and to superimpose flashes detected
158 by the WWLLN during a period (usually 10 minutes) centred on the scan time. The flash rate
159 density (FRD) is calculated by using the flash rate divided by the fractional area $A(\tau)$, usually A(-
160 40°). To analyze the meteorological conditions for both days, we used the Convective Available
161 Potential Energy (CAPE) and humidity values from re-analysis performed by NCEP/NCAR. Thus,
162 we plotted CAPE and humidity at 12:00 UTC for the study area. The tropopause temperatures are
163 also issued from NCEP/NCAR reanalysis.
164
165 3 Results and interpretation
166 3.1 Overall analysis of two active periods
167 Figure 2 illustrates the overall temporal correlation of lightning activity with CAPE, for the
168 months of March and December 2013 with 934,917 and 1,212,071 lightning flashes, respectively.
169 The lightning activity is estimated by the daily number of lightning flashes and the CAPE is
170 considered with the area in which it is greater than a threshold which is 1,000 and 2,000 J kg^{-1} in
171 the graphs 2a and 2b, respectively. The daily CAPE value is considered as the average calculated
172 over three daily values at 00:00, 08:00 and 16:00. We notice that lightning activity is present every
173 day without exception for the two months, but significantly stronger on some days than on others.
174 Thus, the number of flashes varies from 12,712 (March 9) to 81,145 (December 25) flashes per
175 day. It is rather high at the beginning of March and December, rather low in the middle of the two
176 months, then again high around the 20th and on the last days for the month of March, finally on
177 the whole end of December from 20 (Figures 2a and 2b). We also notice that the CAPE fractional
178 area curves follow, to a certain extent, the trend of the evolution of the daily flash rate, especially
179 over certain periods such as the end of December which is a very active period of several days
180 (Figure 2b).
181 The month of March is marked by very high values for the area at 1,000 J kg^{-1} (Figure 2a).
182 These values are around 35×10^5 km^2 at the start of the month and remain greater than or equal to
183 20×10^5 km^2 during the rest of the month except for three days (March 11-13). On the other hand,
184 for the area at 2,000 J kg^{-1} the values generally remain less than or equal to 6×10^5 km^2 except for
185 a small number of days, and particularly for the beginning of the month when values are recorded
186 around 13×10^5 km^2 (Figure 2b). Compared to March, December is marked by relatively lower

187 values of the area at 1,000 J kg^{-1} (Figure 2a). However, values greater than 15×10^5 km^2 are
188 recorded for ten days at the beginning of the month and for more or less seven days at the end. For
189 the area at 2000 J kg^{-1} the values generally remain less than or equal to 2×10^5 km^2 except for a
190 small number of days, mainly at the beginning and at the end of the month, when values are
191 recorded up to 10×10^5 km^2 and around 4×10^5 km^2, respectively (Figure 2b).

192 Figure 2c,d shows the correlation graphs between the two daily parameters analyzed for the
193 two CAPE values. The correlations are positive in all cases, but with relatively average coefficients
194 which does not show a strong correlation over the entire periods considered. In December, the
195 correlations are better, with determination coefficients $R^2 = 0.555$ for 1,000 J kg^{-1} and $R^2 = 0.440$
196 for 2,000 J kg^{-1} (correlation coefficients of 0.745 and 0.663, respectively). Indeed, these
197 coefficients are lower for the month of March, with $R^2 = 0.216$ for 1,000 J kg^{-1} and $R^2 = 0.301$ for
198 2,000 J kg^{-1} (correlation coefficients of 0.465 and 0.549, respectively).

199 Figure 3a,b shows the lightning flash density in the whole study area for March and
200 December with a resolution of $0.1° \times 0.1°$. During the two months examined, the storm occurrence
201 is marked by the large spatial extension of the lightning activity and the storm frequency or
202 intensity by the strong local densities that reach about 3 km^{-2} and 2 km^{-2} in December and March,
203 respectively. Thus, the larger number of flashes in December is translated as larger local densities.
204 The larger values are found in the same area for both months, west of Rwanda in Kivu region, also
205 noted as the main maximum in Kigotsi et al. (2018). It seems this maximum is present at any time
206 scale, annual, seasonal as seen in Soula et al. (2016), or monthly in the present study. Most of other
207 large values are lower and scattered west of this main maximum, for both months but in a more
208 pronounced fashion for December (Figure 3b), to form a secondary region of strong activity, as it
209 was analyzed in Kigotsi et al. (2018) at annual scale. A region of large flash density for both months
210 is observed in the southeastern part of the area, along Malawi Lake. Figure 3c,d displays the
211 thunderstorm initiation which is considered as the occurrence of a flash when no other flash was
212 detected during the previous 30 minutes in a radius of 50 km. The values are low with a maximum
213 of about 2 flashes per 100 km^2 since only the first flash of a thundercell is counted. The density of
214 these "first" flashes is also scattered in the entire study area for the two months, except in its
215 northern part. However, larger values are visible in some regions that are usually east of the large
216 values of the flash density in Figure 3a,b. This observation could support a westerly propagation
217 of storms as usually observed in many studies (e.g. Laing et al., 2011). Indeed, by using Meteosat

observations and reanalysis data, Laing et al. showed the propagation of convective systems and their modulation by Kelvin waves. Looking a little more in detail Figure 3c,d, we can see larger values of density ~~are~~ located in the eastern part of DRC, along the Rift Valley which follows a line with many lakes (Kivu, Tanganyka), in northern Malawi Lake for both months, along the border with Zambia at lake Mweru location. In the western and southwestern parts of the study area, some locations provide large values of the density, especially for March in Cameroon and for both months in south of Gabon (Figure 3c), while other parts in the eastern and southern study area provide also large values in December (Figure 3d).

3.2 Analysis of four active zones

Figure 4 shows the flash density (a, b), the characteristics of CAPE (c, d) and humidity at low level (900 hPa) (e, f) in the whole study area, and for two periods of 24 hours, one in March 4-5 with 50,726 flashes in panels a, c, e, and one in December 25-26 with 72,723 flashes in panels b, d, f. We can see that a large part of the study area is globally affected by thunderstorm activity within 24 hours. Only the northernmost band of the area between 5°N and 10°N latitude, notably on December 25 (Fig. 4b), and the part of the Atlantic Ocean (south-western part of the area) for the two days are not affected by lightning. These two regions also present very low values of CAPE (Fig. 4c-d) while the northern region is concerned by low humidity (Fig. 4e-f). The spots of lightning flash density are generally spread in the other parts of the area, with low values at this scale, generally much less than 1 flash km^{-2} with some areas where this density can locally reach values close to 1 flash km^{-2}, as shown by the black dotted frames for the two days. On March 4, the strong values of lightning density are rather on the eastern half of the area while on December 25 they are located mainly in two equatorial zones around 28°E and 18°E, which correspond to the two zones defined as the main and secondary maximum, respectively, in the statistical study by Kigotsi et al. (2018). One of these regions is common in both days around 27-28°E and 1-3°S, it is the one which corresponds to the main maximum in Soula et al. (2016) and Kigotsi et al. (2018). The CAPE is large within or near these regions of large lightning flash density. For example, the CAPE has values > 3 kJ kg^{-1} on March 4 close to both regions highlighted by the frames M_1 and M_2 (Fig. 4c), while it has values around 3 kJ kg^{-1} close to D_1 and close to 5 kJ kg^{-1} within D_2 on December 25 (Fig. 4d). The relative humidity in Fig. 4e,f corresponds roughly well with the large values of CAPE. These first observations lead us to consider the detail of the lightning densities

(Fig. 5) and the development of activity during the day (section 3.3) in the four areas marked by M_1 and M_2 for March, and D_1 and D_2 for December, in Figure 4a,b.

The density of lightning in M_1 (Fig. 5a) including 3,293 flashes is globally distributed over the 3° × 3° area with two regions of higher density, one lying east-west between 26°E and 27°E and between about 8.6°S and 9°S, the other in a spot at 26°E and 8°S. The first region has a maximum of about 0.8 flash km^{-2} and the second 0.6 flash km^{-2} much more concentrated. In M_2 (Fig. 5b) including 6,339 flashes, the density of lightning is both higher with a maximum close to 1 flash km^{-2} and more spread with several cores at more than 0.6 flash km^{-2}. For December 25 the regions of high activity are presented in Fig. 5c,d. The first with 8,274 flashes is similar to the second of March 4, in maximum value (~ 1 flash km^{-2}) and in location (around 27°E-28°E and 2°S-3°S). The second one, located more to the west is much more spread out with 30,481 flashes in 24 hours and a great number of cores at values of about 1 flash km^{-2} spread over an area of 5° × 5°. In all cases, the large values of the lightning flash density are localized in small regions, at about the size of the spatial resolution of 0.1°, which represents about 10 km within the study area. To well understand the shaping of these spots during the storm activity, we analyze in the following and for each, the time evolution and the location of the flashes, as well as that of the cloud structure thanks to the temperature of its top.

3.3 Case studies of storm systems

Storm system M_1

Figure 6a displays the time series of different parameters of the storm activity (flash rate, flash rate density FRD(-40°), fractional areas of CTT, min(CTT) and Figure 6b-e shows maps of CTT with flashes detected over 10 minutes. The storm in M_1 occurred at the beginning of the night of March 4 around 19:45 UTC (21:45 local time) and at about 26.5°E and 8.5°S. It corresponds to the National Park of Upemba within Katanga region, southeastern DRC, an area with many lakes (Kabwe, kabele, Mulenda, Upemba, Kisale, Kabamba…) at an altitude between 600 and 700 m surrounded by several plateaus with altitudes above 1,000 meters. The storm system exhibited two convective cores, the first that developed between 19:45 and 21:00 UTC with min(CTT) of -94°C and a flash rate of 15 flashes min^{-1} at 21:00 UTC (Figure 6a,b), and the second one that developed about one hour later (Fig. 6a,c). The CTT values were colder with a minimum of -95.6°C at 21:45 UTC, but the flash rate reached the same maximum value of 15 flashes min^{-1} at that time while the

first core was still active (Figure 6a,d). The system developed in size after 21:45 UTC while the fractional area of coldest CTT A(-80°) and the flash rate decreased (Figure 6a,e). The storm system size A(-40°) reached a maximum of 52,000 km^2 at 00:30 during a long dissipation phase. FRD (-40°) was correlated to the flash rate for this storm and reached a maximum at 21:00 UTC when the first core was very active. The flashes were mainly located within the coldest cloud top areas during the active phase of the storm. The storm did not move during its lifetime, which makes a short duration of activity without any regeneration of cell and a characteristic of isolated thunderstorm that developed in an area with spots of CAPE > 3 kJ kg^{-1} (Figure 4c).

Storm system M_2

The characteristics of storm M_2 are shown in Figure 7 as in Figure 6 for M_1. This storm developed at the beginning of the night of March 4th in the region of the main maximum of storm activity observed by Soula et al. (2016). The first flashes were detected around 22:00 UTC in the region of Virunga mountain range that reaches about 3,000 m of height. The storm took the structure of an MCS over a few hours with a convective line including several cores that moved westerly with a velocity of about 40 km h^{-1}, and a rear stratiform region, well visible in Figure 7b-g. The flash rate increased progressively during this development and reached the maximum of 35 flashes min^{-1} at 01:00 UTC, while min(CTT) was -94.75°C. After this maximum, the flash rate decreased and fluctuated following new cell developments while the CTT was minimum at 01:45 UTC with -96.6°C. The last cell development was at 03:00 UTC with a minimum CTT of -94.75°C, before the maximum extent of the system around 04:30 UTC with a fractional area A(-40°) of 72,000 km^2. The strongest flash increase during this storm was observed between 00:00 and 01:00 UTC, simultaneously to a fast decrease of min(CTT), when several cells seemed to merge in the main core of the convective region (Figure 7d,e). Most flashes were located at the front of the convective region, forming clusters corresponding to each cell.

Storm system D_1

The storm system D_1 is described in Figure 8 with the same parameters as the previous cases. This storm still developed in the main maximum region highlighted in Soula et al. (2016), a little more north and earlier in the afternoon than the system M_2. Indeed, the first flashes were recorded around 16:00 UTC at about 28°E and 1°S, in a region that corresponds to the forest at an altitude

311 of about 1,000 m in the National Park of the Maiko. The flash rate exhibited a first peak at about
312 17:30 UTC with 10 flashes min^{-1} while min(CTT) was -89.7°C. At that moment the storm consisted
313 of two convective areas producing flashes as indicated in Figure 8b. The two convective areas
314 exhibited a strong decrease of activity until 18:00 UTC followed by a very fast regeneration of
315 cells from the most southern one (Figure 8a,c) resulting in a very fast increase of the flash rate up
316 to 18.7 flashes min^{-1} at 19:00 UTC and a very rapid decrease of CTT from -84°C at 18:00 UTC to
317 -92°C at 18:45 UTC. During one more hour the flash rate decreased again and restarted to increase
318 between 20:00 and 21:30 UTC to reach 21 flashes min^{-1} when the two initial convective areas
319 merged around 20:00 UTC and three cores developed within this new convective structure. The
320 CTT exhibited minimum values of -92°C and -93°C at 18:45 and 21:15 UTC, respectively. The
321 system continued to produce flashes during a few hours, while maintaining its structure with three
322 convective cores, the CTT of which became less and less cold (Figure 8a,d,e). The majority of
323 flashes were produced after 20:00 UTC which corresponds with the merged convective areas. This
324 storm occurred in a region with CAPE values around 2 or 3 kJ kg^{-1} as indicated in Figure 4d, i.e.
325 lower than the previous storm cases, which can explain less cold CTT values. The size of the system
326 A(-40°) reached about 65,000 km^2 after the main lightning activity at about 23:30 UTC and before
327 to decrease progressively.
328
329 *Storm system D_2*
330 This storm occurred on December 25th in a region of very large CAPE values, close to 5 kJ
331 kg^{-1} as indicated in Figure 4d. Figure 9 displays the characteristics of this activity during a long
332 period of 14h 30min and within an area of 6° × 6°. The first flashes within the area occurred early
333 in the afternoon, and their rate increased during a few hours until 20:00 UTC to reach 83 flashes
334 min^{-1}. Several convective areas produced these flashes, as indicated in Figure 9b,c at 14:00 and
335 16:00 UTC, respectively. These convective areas grew and moved slowly southwards as shown by
336 the successive panels of Figure 9. The min(CTT) reached a minimum of -96.6°C two times during
337 the episode, at 20:30 and 22:30 UTC and the area A(-40°C) increased up to 300,000 km^2 with
338 especially large areas of A(-80°), in red in Figure 9a. Even if the flash rate increased during a few
339 hours, FRD(-40°) decreased and staid approximately constant during the beginning and the
340 development of the storm, respectively. Thus, the maximum value of FRD was 0.019 flash km^{-2} h^{-1}
341 when the flash rate was maximum at 20:00 UTC, which corresponded to a lower value than for

the previous cases, especially those of March 4th displayed in Figures 6 and 7. The flash rate increase was due to ~~the developments of~~ intramass convective cells which developed within large cloud areas with CTT < -40°C. The proportion of areas with cold CTT was much larger than in the previous cases but the convective cores did not represent large parts of these areas. Globally, the storm was not very efficient to produce lightning flashes, in spite of large areas of clouds with very cold CTT values. The region also contains some lakes such as Maindombe (18.20°E; 1.88°S) and Tumba (18.0°E; 0.76°S), and it is crossed by the Congo river which is very wide there. Furthermore, its lower troposphere contains large values of humidity on that day as shown in Figure 4f. There is for example a good correspondence between the area of the two lakes and the location of the strong activity around 20:00 UTC (Figure 9f), when the flash rate is maximum (Figure 9a). Probably, there were regeneration of the storm system above these two lakes, while propagating.

3.4 Daily cycle

Figure 10a represents the evolution of thunderstorm activity over the whole study area and for the period from December 27, 2013 at 04:00 UTC to December 29, 2013 at 00:00 UTC. This activity is expressed by the variation of the fractional areas of the cloud tops at different temperature ranges, as well as those of min(CTT), the lightning flash rate and FRD(-40°). It is observed that the colder surfaces of the cloud tops describe a diurnal cycle, evidenced for the 2-day duration, of which the minimum and the maximum appeared at the same time, between 07:00 and 08:00 UTC and between 15:30 and 16:00 UTC, respectively. However, the maximum value of the total area A(-40°C) was much larger on December 28, 2013 (~162×10^4 km^2) compared to December 27, 2013 (~105×10^4 km^2). The remarkable difference between the two maximums (ratio of around 1.5) was mainly due to the areas with cold CTT but not the coldest ones. Indeed, the maximum of A(-80°C) was 3.1×10^4 km^2 and 2.6×10^4 km^2 for 27 and 28 December maximums, respectively. For A(-75; -80°C), a larger maximum was observed on 28 December, with a value of 11×10^4 km^2 compared to 6.5×10^4 km^2 for 27 December. The flash rate described the same daily cycle, but its maximum usually preceded that of the total fractional area A(-40°C) by at least one hour. This time lag is natural because the maximum of the total area depends on the phase of thunderstorms that have occurred in the area, and it is maximum during their dissipation, while the maximum of the lightning flash rate is related to the mature phases of these thunderstorms. Indeed, the flash rate maximum was better correlated in time with the maximum of the coldest fractional areas, rather than the total fractional areas: it was maximum on December 27 at 15:00 (about one hour before A(-40°)) and 16:30 UTC with a value of about 65 flashes per minute, and it was maximum on December 28 at 14:15 UTC (more than one hour before A(-40°)) with a value of 74 flashes per minute. The flash rates were therefore more correlated with the

coldest cloud tops areas, since the ratio 1.5 found for the total fractional areas is not confirmed for the flash rates. Indeed, the ratio for A(-80°) was 0.84 between December 28 and 27. The difference can be interpreted in terms of the extent of MCSs involved in the overall two-day storm activity and by the way, the overall area A(-40°) was much larger at the beginning of the second day (47×10^4 km^2 at 07:30 UTC) than at that of the first day (25×10^4 km^2 at 07:30 UTC). On the other hand, if we assume that the average size of an MCS involved in this activity was of the order of 60×10^3 km^2, an average value that would take into account the sizes of the storm systems described in section 3.3 (M_1, M_2 and D_1), the maximum values for the whole area would correspond to approximately 17 systems on December 27, and 26 systems on December 28. However, the flash rates did not confirm the activity corresponding to such ratio and therefore, it means the systems were more extended and started earlier on December 28 and all could not be considered as being MCSs.

Furthermore, this interpretation also accounts for the contrast observed between the spatial lightning density distributions represented in Figure 10b,d. As the presence of lightning provides information on that of thunderstorms, the dispersion characterizing the flash density for the periods 08h00-20h00, December 27 (Figure 10b) and 08h00-22h00, December 28 (Figure 10d) indicates that during these time intervals the storm systems were numerous and scattered over a large part of the study area. However, the large values of density, typically around 1 flash km^{-2}, were not numerous, which confirms a low number of systems as those analyzed in section 3.3. On the other hand, the thunderstorm activity exhibited another maximum during the period from 20:00 and 06:00 UTC on December 27-28, with a maximum of 74.5 flashes min^{-1} at 02:30 UTC and a maximum of 60×10^4 km^2 for A(-40°) at the same time (Figure 10a). FRD was much larger at that moment than during the day-time maximum and the fractional area A(-80°) is also large during the period with values around 2×10^4 km^2, which means the storm activity was less scattered. Figure 10c confirms the lightning flashes were less scattered and therefore produced by less numerous systems. Furthermore, a large proportion of flashes were produced west of Rwanda and Kivu Lake, where the main maximum of storm activity was reported in several studies, especially in Soula et al. (2016). These authors showed that this maximum, present at any period of the year, is due to more frequent storms, and furthermore these storms are probably either more active or more stationary or more extended, than elsewhere in the study area. The values of min(CTT), reported every fifteen minutes in Figure 10a, ranged between -77°C and -96°C, when lightning activity was observed. It fluctuated much because of several storm systems that could reach their maximum vertical development at different times. Lightning flash rate and minimum temperature varied in opposite sense, so that colder temperatures were associated with higher lightning rates.

4. Discussion

During two periods of one month (March and December 2013) selected for their strong lightning activity, we analyze the correlations between the number of flashes, the CAPE and the cloud characteristics. Lightning flashes were produced for all the days from these two months, including between 12,712 and 81,145 flashes per day. First over each of the months, we find a correlation between the fractional area for two values of the average daily CAPE (1 and 2 kJ kg^{-1}) and the number of flashes. Four correlation coefficients were calculated for the distribution according to the month and the CAPE value: the greatest is 0.745 for a CAPE value of 1 kJ kg^{-1} and the month of December, while the lowest is 0.465 for a CAPE of 1 kJ kg^{-1} and the month of March. For both CAPE values, the correlation is better for the month of December. These coefficients do not show a very strong correlation and therefore these two parameters are not perfectly correlated. The average daily flash number was 30,158 for March and 41,795 for December while the average daily areas for CAPE > 1 kJ kg^{-1} was 27.7×10^5 km^2 for March and 15.46×10^5 km^2 for December. For CAPE > 2 kJ kg^{-1} it was 38.60×10^4 km^2 and 19.99×10^4 km^2 for March and December, respectively. Thus, the number of flashes is larger in December while the area for both CAPE values is lower. It means clearly that the fitting provides different relationships for the two months when considering the area of CAPE values. Even if several studies of tropical storms have shown that the flash rate tends to be larger on days with large CAPE values (Williams et al., 1992; Petersen et al., 1996), other parameters as for example the CAPE cycle of decreasing and increasing can affect the lightning activity (Williams et al., 1992). Furthermore, we find different relationships between daily CAPE and flash number for the two months considered, with larger values of flash number for a same area with large CAPE in March compared to December. It means there is a seasonal effect of the CAPE on lightning activity. This effect can be linked to other parameters, as for example the concentration of aerosol particles and the microphysics that could contribute to deep convection in the Congo Basin. Indeed, Sherwood et al. (2006) proposed the regulatory mechanism of water and ice content in the troposphere of equatorial Africa by involving aerosols. Thus, they showed that the maximums in lightning activity in the Congo Basin are associated with small effective diameters of ice crystals near the top of the cumulonimbus cloud and that the highest thunderstorms produce the smallest effective diameters of ice crystals. Several studies have attributed the reduction in these effective diameters of ice crystals, gathered within the vicinity of the top of the cumulonimbus, to large amounts of atmospheric aerosol particles (Sherwood, 2002a,b; Ekman et al., 2004). Furthermore, as Sherwood et al. (2006) suggested that

extensive biomass burning may play a role in intensifying thunderstorms, deep convection can also be enhanced by extensive biomass burning in the equatorial forest sector of the Congo Basin. It can be noted that the point of view of Sherwood et al. corroborates with studies that have reported the existence of an influence of smoke released into the atmosphere by anthropogenic forest fires on the increase or decrease in thunderstorm intensity (Altaratz et al., 2010).

Two periods of 24 hours (from 06:00 to 06:00 UTC the next day) with strong activity, one for each month, have been selected to make the comparison of the spatial distribution of CAPE with the lightning flash density. It shows the high values of lightning flash density are restricted to very small areas while the CAPE spread on very large ones. Generally, large CAPE values do not systematically correspond to high values of flash density, although the flashes are produced in areas with large CAPE values around. It must be concluded that the strong ascents of air masses to generate thunderstorms that are necessary to produce lightning flashes, are possible thanks to large CAPE values but the displacement of the storm during its development can shift the accumulation of lightning flashes. The intensity of these storms does not only depend on dynamics and thermodynamics conditions. Indeed, as already indicated in this section, the production of lightning by thunderstorm systems is strongly conditioned by microphysical characteristics (Takahashi, 1978; Saunders et al., 1991) and thus, the imperfect correlation observed can be explained.

The approach consisting in looking at the first flash produced by a storm indicates a larger density of storm triggering in regions with lakes and/or mountains. The study by Laing et al. (2011), devoted to the analysis of the cycles and propagation of deep convection in equatorial Africa during the period 2000-2003, also highlighted the influence of the mountains surrounding the Rift Valley, especially for mesoscale convective systems that propagate mainly westward. In addition, the authors mainly identified two sources of moisture namely Lake Victoria and Lake Tanganyika (Laing et al., 2011). The role of orography or lakes in the development of thunderstorms and the distribution of lightning has been pointed out by several researchers in other parts of the world (Oki and Musiake (1994) in Japan, Hodanish et al. (1997) in Florida, Yang and Slingo (2001) in the tropics, Pujol et al. (2011) in Europe). For example, Pujol et al. describe and quantify the microphysical processes involved in the initiation and development of convective precipitation resulting from orographic effects in the presence of a lake. They noted that the lake can act as a secondary source of moisture that can promote local convection, and the mountainous slopes will promote updrafts.

We have analyzed four specific activities by considering the CTT and the flash rate, as well as parameters derived from both. Different types of storms are included in the areas where these activities developed, from the cell with a unique convective core active, to the MCS and the intramass storms covering large areas. Table 1 shows the characteristics of each and their environment. These storm sequences occurred in areas with CAPE values up to 3 kJ kg^{-1} in part of them on March 4th. For December 25th, the CAPE reached also about 3 kJ kg^{-1} in the region of the storm system D_1 and between 4 and 5 kJ kg^{-1} in a large part of the region of the system D_2. We analyzed the temperature of the tropopause in the region of each system and plotted it for both days in Figure 11a,b. This temperature was substantially colder on March 4, with a minimum of -84°C in the region of M_2 and -82°C in the region of M_1. It was -81°C and -80°C for D_2 and D_1, respectively, on December 25th. According to the values reached by min(CTT) during the storms, we can say the stronger the CAPE, the higher the development of the cloud above the tropopause. Indeed, the difference between min(CTT) and $T_{tropopause}$ is greater for strong CAPE, as indicated in the fifth column of Table 1. The large values of CAPE lead to strong convection and large vertical development of the clouds. The vertical velocity within the convective clouds is linked to the CAPE:

$$w = (2 \times CAPE)^{1/2}$$

Because the strength of the updraft is maximum at the equilibrium level (the tropopause level), the cloud air continues to rise because of its own upwards momentum, until the negative buoyancy due to the parcel finding itself colder than its surroundings. Thus, the overshoot develops above the tropopause which makes much colder CTT compared to the tropopause. The maximum height of the overshoot is observed for D_2 with a CTT of -15.6°C colder than the tropopause as indicated in Table 1. It corresponds to a height of about 1.5 km above the tropopause, according to the adiabatic transformation temperature cooling rate (-9.8° km^{-1}) which can be considered for cloudy air rising at this altitude (Jacobson, 2005). In each of the four cases, the thundercloud reached more than 1 km above the tropopause since the minimum was found for M_2 at about 1.2 km. Figure 12 displays the values of the maximum height of the cloud versus the CAPE values found in the storm area, for the small sample of storm cases. The curve fitting provides a very high determination coefficient (r^2 = 0.984), which shows a very tight relationship between both parameters. These large overshoots make wide areas with cold temperature in D_2 but the flash rate density is the lowest among the four cases. The highest FRD value is found for the system M_2

501 which is an organized system that can be considered as an MCS with several convective cores
502 simultaneously active. The organization of a storm system allows more flashes to be produced at
503 the same time.

504 During the storm activity of all four cases, the maximum flash rate corresponded with the
505 minimum of the CTT in timing, especially for the cases with only one cell (M_1) or several cells
506 imbedded in the same cloud system (M_2 and D_1). For the case with several intramass convective
507 cores, the simultaneity of both is less visible. On the other hand, for all cases a very large majority
508 of the flashes were associated with the coldest CTT regions which were also the convective cores.
509 This observation is typical of what is obtained in the experiments with lightning mapping and
510 thundercloud detection, as for example in Carey et al. (2005). By using a Lightning Detection and
511 Ranging (LDAR II) and radar data, these authors showed that an overwhelming majority of VHF
512 sources radiated by flashes during the lifetime of a leading-line, trailing-stratiform (LLTS) MCS,
513 were located within the convective region. Our observations show that the clusters of flashes
514 associated with the convective cores develop before the thundercloud reaches its maximum height
515 and therefore can be used as a proxy to locate the convective cores. Other observations in the
516 literature show clearly the correspondence between the lightning clusters and the strong convective
517 cores (Dotzek et al., 2005; Soula et al., 2014). On the other hand, the CTT can be very cold without
518 any lightning flash detected or very few, as in many locations of D_2. Thus, the lightning location
519 in real time, simultaneously to the CTT observation as it is made currently by GLM on GOES
520 (Goodman et al., 2013) and as it will be made by LI on MTG satellite, especially over Africa
521 (Dobber and Grandell, 2014), is a good complement for a better nowcasting of storms (Rudolsky
522 et al., 2018; Rudlosky and Virts, 2021).
523
524 5. Conclusion

525 The lightning activity observed by the WWLLN within a large area of Central Africa (25°
526 × 25°) is analyzed for two one-month periods of 2013 with a large amount of lightning flashes, as
527 well as the associated meteorological and environmental conditions. The sample of data used in
528 the analysis has been chosen to be representative as much as possible of a strong lightning activity.
529 Thus, among the database from WWLLN available, we choose the year with the best detection
530 efficiency and two months with high level of lightning activity and low variability from one year
531 to the next. A correlation is found between the daily flash number and the extent of large CAPE

values. However, the correlation coefficients are not very high over the whole period of the study. There is a seasonal effect on the number of flashes produced by storms with the same extent of large CAPE values. There were also large values of moisture in the lower layers of the troposphere in the days with a strong lightning activity. The lightning flash density distribution for each period of one month shows the same location for the maximum, which corresponds with the main maximum reported in the literature for annual activity, with about 3 and 2 flashes km^{-2} for December and March, respectively. The storms developments characterized by the first flash detected often occur in the regions that combine the presence of lakes and mountains, which shows the role of the relief for triggering convection.

The detailed analysis of the lifecycle of several convective systems shows a very good spatial and temporal correlation of the flash production and the convective core developments. The flash rate density is larger in the convective systems well organized, as the typical MCS. It is also larger during the development of the storms and when several cells merge. The flash clusters allow to localize the strong convective activity and to follow the displacement of the storm systems when they move. The analysis of a period of two days in December over the whole study area, shows the daily cycle with a lightning flash rate maximum between 14:00 and 15:00 UT that precedes the maximum development of the storm by one hour. The minimum occurs between 07:00 and 08:00 UT. The daily cycle also shows that the storms located within the region of the main maximum of lightning activity are more frequent and produce larger values of the flash rate density.

The approach of the present study consisted in selecting periods with high lightning activity in the Congo Basin. According to the processes leading to the lightning flash depend on many parameters (microphysics and aerosol particles, dynamics within the cloud, ice content in the mixed layer, warm cloud depth…) another approach will be to consider widely cases with different conditions. The goal of such studies is to optimize the use of lightning information for nowcasting applications and understanding of storm developments.

Acknowledgments

The authors thank the World-Wide Lightning Location Network (http://wwlln.net/) and Christelle Barthe from University of la Réunion (France) for providing the lightning location data used in this study. They thank the French AERIS/ICARE Data and Services Center which provided MSG/SEVIRI data for cloud top temperature. They thank also the European Copernicus/ECMWF

563 Data Center, the US NCEP/NCAR and NOAA for providing meteorological reanalysis. JK is
564 grateful to the French "Ministère des Affaires Etrangères", to the French Embassy in DRC, for
565 supporting his stay in France and "Groupe International de Recherche en Géophysique
566 Europe/Afrique" (GIRGEA) for cooperation organisation, especially Christine Amory.

567

568 References

569 Abarca, S.F., Corbosiero, K.L., 2011. The World Wide Lightning Location Network and
570 convective activity in tropical cyclones. Mon. Wea. Rev. 139, 175–191.

571 Albrecht, R., Goodman, S., Buechler, D., Blakeslee, R., Christian, H., 2016. Where are the
572 lightning hotspots on Earth? Bull. Amer. Meteor. Soc. 97, 2051-2068. doi : 10.1175/BAMS- D-
573 14- 00193.2.

574 Altaratz, O., Koren, I., Yair, Y., Price, C., 2010. Lightning response to smoke from
575 Amazonian fires. *Geophys. Res. Lett., 37*(L07801). doi:10.1029/2010GL042679.

576 Ba, M.B., Nicholson, S.E., 1998. Analysis of convective activity and its relationship to the
577 rainfall over the Rift Valley Lakes of east Africa during 1983–90 using the Meteosat infrared
578 channel. J. Appl. Meteorol. 37, 1250–1264.

579 Carey, L.D., Murphy, M.J., McCormick, T.L., Demetriades, N.W.S., 2005. Lightning
580 location relative to storm structure in a leading-line, trailing-stratiform mesoscale convective
581 system, J. Geophys. Res., 110, D03105, doi:10.1029/2003JD004371.

582 Cecil, D., Buechler, D.E., Blakeslee, R.J., 2014. Gridded lightning climatology from TRMM-
583 LIS and OTD: Dataset description. Atmos. Res. 135, 404–414. http://. dx.doi.org/
584 10.1016/j.atmosres.2012.06.028.

585 Christian, H.J., Blakeslee, R.J., Boccippio, D.J., Boeck, W.L., Buechler, D.E., Driscoll, K.T.,
586 Goodman, S.J., Hall, J.M., Koshak, W.J., Mach, D.M., Stewart, M.F., 2003. Global frequency and
587 distribution of lightning as observed from space by the Optical Transient Detector. J. Geophys. Res.
588 108(D1), 4005. http://. dx.doi.org/ 10.1029/2002JD002347.

589 Dai, A., 2001. Global precipitation and thunderstorms frequencies. Part II: Diurnal
590 variations. J. climate. 14, 1112-1128.

591 Dai, A., Giorgi, F., Trenberth, K.E., 1999. Observed and model simulated diurnal cycles of
592 precipitation over the contiguous United States. J. Geophys. Res. 104, 6377-6402.

593 Dobber, M., Grandell, J., 2014. Meteosat Third Generation (MTG) Lightning Imager (LI)
594 instrument performance and calibration from user perspective. Proceedings of the 23rd Conference
595 on Characterization and Radiometric Calibration for Remote Sensing (CALCON), 11-14 August
596 2014, Utah State University, Logan, Utah, USA.

597 Dotzek, N., Rabin, R.M., Carey, L.D., MacGorman, D.R., McCormick, T.L., Demetriades,
598 N.W., Murphy, M.J., Holle, R.L., 2005. Lightning activity related to satellite and radar
599 observations of a mesoscale convective system over Texas on 7–8 April 2002. Atmos. Res. 76,
600 127–166.

601 Dowden, R.L., Brundell, J.B., Rodger, C.J., 2002. VLF lightning location by time of group
602 arrival (TOGA) at multiple sites. J. Atmos. Solar-Terr. Phys. 64, 817-830.

603 Ekman, A.M., Wang, C., Wilson, J., Strom, J., 2004. Explicit Simulations of aerosol physics
604 in a cloud-resolving model: A sensitivity study based on an observed convective cloud. Atmos.
605 Chem. Phys., 4, 773-791.

606 Farnsworth, A., White, E., Williams, C.J.R., Black, E., Kniveton, D.R., 2011. Understanding
607 the large Scale Driving Mechanisms of Rainfall Variability over Central Africa. Advances in
608 Global Change Research. *43*. doi:10.1007/978-90-481-3842-5_5

609 Goodman S.J., Blakeslee R.J, Koshak W.J., Mach D., Bailey J., Buechler D., Carey L.,
610 Schultz C., Bateman M., McCaul Jr. E., Stano G., 2013. The GOES-R Geostationary Lightning
611 Mapper (GLM). Atmos. Res., 125–126, 34–49, doi:10.1016/j.atmosres.2013.01.006.

612 Hodanish, S., Sharp, D., Collins, W., Paxton, C., Orville, R.E., 1997. A 10-yr monthly
613 lightning climatology of Florida: 1986–95. Weather Forecast. 12, 439–448.

614 Jackson, B., Nicholson, S., Klotter, D., 2009. Mesoscale convective systems over western
615 equatorial Africa and their relationship to large-scale circulation. Monthly Weather Review. 137,
616 1272-1294. doi: 10.1175/2008MWR2525.1.

617 Jacobson, M. Z., 2005. Fundamentals of atmospheric modeling (2nd edition) (2nd ed., Vol.
618 9780521839). Cambridge University Press. doi:10.1017/CBO9781139165389.

619 Kigotsi, J.K., Soula, S., Georgis, J.-F., 2018. Comparison of lightning activity in the two
620 most active areas of the Congo Basin. Natural Hazards and Earth System Sciences. 18, 479-489,
621 2018. http://.doi.org/10.5194/nhess-18-479-2018.

622 Laing, A.G., Carbone, R.E., Levizzani, V., 2011, Cycles and propagation of deep convection
623 over equatorial Africa. Monthly Weather Review. 129, 2832-2853.

624 Laing, A. G., Carbone, R. E., Levizzani, V., Tuttle, J. D., 2008. The propagation and diurnal
625 cycles of deep convection in northern tropical Africa. Quart. J. Roy. Soc. 134, 93-109.

626 Liu, C., Zipser, E.J., 2005. Global distribution of convection penetrating the tropical
627 tropopause. J. Geophys. Res. 110, D23104. doi: 10.1029/2005JD006063.

628 Mohr, K.I., Thorncroft, C.D., 2006. Intense Convective Systems in West Africa and their
629 relationship to the African easterly jet. Quart.J.Roy.Meteor.Soc. 132, 163-176.

630 Nguyen, H., Duvel, J.-P., 2008. Synoptic wave perturbations and convective systems over
631 equatorial Africa. J. Climate. 21, 6372–6388.

632 Nicholson, S., Grist, J.P., 2003. On the seasonal evolution of atmospheric circulation over
633 West Africa and equatorial Africa. J. Climate. 16, 1013–1030.

634 Oki, T., Musiake, K., 1994. Seasonal change of the diurnal cycle of precipitation over Japan
635 and Malaysia. J. Appl. Meteor. 33, 1445-1463.

636 Petersen, W.A., Rutledge, S.A., Orville, R.E., 1996. Cloud-to-ground lightning observations
637 from TOGA COARE: Selected results and lightning location algorithms. *Mon. Weather Rev., 124*,
638 602-620.

639 Pujol, O., Lascaux, F., Georgis, J.-F., 2011. Kinematics and microphysics of MAP-IOP3
640 event from radar observations and Meso-NH simulations. Atmos. Res., 101, 1–2, 124–142.

641 Rodger, C.J., Brundell, J.B., Holzworth, R.H., Lay, E.H., 2008. Growing Detection
642 Efficiency of the World-Wide Lightning Location Network. Am. Inst. Phys. Conf. Proc., Coupling
643 of thunderstorms and lightning discharges to near-Earth space: Proceedings of the Workshop, Corte
644 (France), 23-27 June 2008, 1118, 15-20, doi:10.1063/1.3137706.

645 Rodger, C.J., Brundell, J.B., Hutchins M., Holzworth, R.H., 2014. The world-wide lightning
646 location network (WWLLN): Update of status and applications. 29th URSI General Assembly and

Scientific Symposium (URSI GASS), Beijing (P. R. of China), 16-23 August 2014.

Rudlosky, S.D., Goodman, S.J., Virts, K.S., Bruning, E.C., 2018. Initial geostationary lightning mapper observations. *Geophysical Research Letters*, *45*. https://doi.org/10.1029/

2018GL081052.

Rudlosky, S.D., Virts, K.S., 2021. Dual Geostationary Lightning Mapper Observations, Mon. Weath. Rev., 149, 4, pp 979-998. https://doi.org/10.1175/MWR-D-20-0242.1

Saunders, C.P.R., Keith, W.D., Mitzeva, R.P., 1991. The effect of liquid water on thunderstorm charging. J. Geophys.R.es. 96(11), 007-11,017.

Sherwood, S.C., 2002a. Aerosols and ice particle size in tropical cumulonimbus. J. Clim., 15, 1051–1063.

Sherwood, S.C., 2002b. A microphysical connection among biomass burning, cumulus clouds, and stratospheric moisture. Science, 295, 1271–1275.

Sherwood, S.C., Vaughan, T.J.P., Wettlaufer, J.S., 2006. Small ice crystals and the climatology of lightning. Geophys. Res. Lett. (33), L05804, doi:10.1029/2005GL025242.

Soula, S., Kigotsi, J.K., Georgis, J.-F., Barthe, C., 2016. Lightning climatology in the Congo Basin. Atmospheric Research. http://dx.doi.org/ 10.1016/j.atmosres.2016.04.006.

Soula, S., Iacovella, F., van der Velde, O., Montanya, J., Fullekrug, M., Farges, T., Bor, J., Georgis, J.-F., NaitAmor, S., Martin, J.-M., 2014. Multi-instrumental analysis of large sprite vents and their producing storm in southern France. Atmospheric Research 135-136, 415-431, doi: 10.1016/j.atmosres.2012.10.004.

Stuhlmann, R., Rodriguez, A., Tjemkes, S., Grandell, J., Arriaga, A., Bézy, J.-L. Aminou, D., Bensi, P., 2005. Plans for EUMETSAT's Third Generation Meteosat geostationary satellite program, Adv. Space Res. 36, 975–981. http://doi.org/10.1016/j.asr.2005.03.091, 2005.

Takahashi, T., 1978. Riming electrification as a charge generation mechanismin thunderstorms. J. Atmos.Sci., 35, 1536-1548.

Torancinta, E.R., Zipser, E.J., 2001. Lightning and SSM/I-Ice-Scattering Mesoscale Convective Systems in the Global Tropics. Journal of Applied meteorology. 40, 983-1002.

674 Wallace, J.M., 1975. Diurnal variations in precipitation and thunderstorm frequency over the
675 conterminous united states. Mon. Wea. Rev. 103, 406-419.

676 Wang, K.Y., Liao, S.A., 2006. Lightning, radar reflectivity, infrared brightness temperature
677 and surface rainfall during the 2-4 July 2004 severe convective system over Taiwan area. J.
678 Geophys. Res. DO5206. doi: 10.1029/2005JD006411.

679 Williams, E.R., Weber, M.E., Orville, R.E., 1989. The relationship between lightning type
680 and convective state of thunderclouds. J. Geophys. Res., 94, 13,213– 13,220.

681 Williams, E.R., Rutledge, S.A., Geotis, S.G., Renno, N., Rasmussen, E., Rickenbach, T.,
682 1992. A radar and electrical study of tropical "hot towers". J. Atmos. Sci., 49, 1386–1395.

683 Yang, S., Smith, E.A., 2006. Mechanisms for diurnal variability of global tropical rainfall
684 oberved from TRMM. J. Climate. 19, 5190-5226.

685 Yang, G.Y., Slingo, J., 2001. The diurnal cycle in the Tropics. Mon. Wea. Rev. 129, 784-
686 801.

687 Zipser, E., Cecil, D., Liu, C., Nesbitt, S., Yorty, D., 2006. Where are the most intense
688 thunderstorms on Earth? Bull. Amer. Meteor. Soc., 1057-1071. doi: 10.1175/BAMS-87-8-1057.
689
690
691 Table 1. Characteristics of the atmosphere in the environment of the storm systems
692 analyzed: max(CAPE) for the maximum value before the storm development; $T_{tropopause}$ for the
693 temperature of the tropopause; min(CTT) for the coldest CTT during the storm system lifetime;
694 min(CTT) - $T_{tropopause}$ for the difference between both temperatures; max(FR) for the maximum of
695 the flash rate during the storm; FRD(-40°) for the flash rate density in the area with CTT < -40°C
696 at the maximum flash rate; A(-80°) for the fractional area with CTT < -80°C.
697

Storm system	max(CAPE) (kJ kg^{-1})	$T_{tropopause}$ (°C)	min(CTT) (°C)	min(CTT) - $T_{tropopause}$ (°C)	max(FR) (min^{-1})	FRD(-40°) (km^{-2} h^{-1})	A(-80°) (km^2)
M_1	3.3	-82	-95.6	-13.6	15	51.2×10^{-3}	4.7×10^3
M_2	2.9	-84	-96.6	-12.6	35	75.9×10^{-3}	5.4×10^3
D_1	3.1	-80	-93.0	-13	21	24.6×10^{-3}	7.3×10^3
D_2	4.8	-81	-96.6	-15.6	83	20.6×10^{-3}	29.5×10^3

698 Figure caption

699

700 Figure 1. Map of Africa with relief, lakes and rivers. The red frame shows the 25° × 25° study area
701 including the whole Democratic Republic of Congo, some countries around, the Basin of Congo
702 and the Great Rift Valley. The colored scale shows the altitude in meter.

703

704 Figure 2. Evolution of the daily lightning flash number and the fractional area for two CAPE
705 average values, 1,000 J kg^{-1} (a) and 2,000 J kg^{-1} (b) over the whole study area and for the months
706 of March and December 2013. Diagram of correlation of the flash number with both fractional
707 areas, for 1,000 J kg^{-1} (c) and 2,000 J kg^{-1} (d) and for both months.

708

709 Figure 3. Lightning flash density at a resolution of 0.1° × 0.1° over the whole study area and for
710 the months of March (a) and December 2013 (b). Density of first flashes within 50 km in radius
711 and after 30 minutes, with the same resolution (0.1° × 0.1°) for March (c) and December (d) in
712 2013, with a unit in number per 100 km^{-2}.

713

714 Figure 4. Lightning flash density at a resolution of 0.1° × 0.1° over the whole study area, (a) for 4-
715 5 March 2013 (06h00-06h00 UT) and (b) for 25-26 December 2013 (06h00-06h00 UT). The frames
716 indicate the four regions where the storm activity is analyzed in detail. Distribution of CAPE values
717 at 12h00 UT, at a resolution of 0.25° × 0.25°over the study area, (c) for 4 March 2013 and (d) for
718 25 December 2019. (e) and (f) same as (c) and (d) for the relative humidity at 900 hPa level.

719

720

721 Figure 5. Lightning flash density at a resolution of 0.1° × 0.1° over the four regions indicated in
722 the frames of Figure 4a,b: a) for M_1, b) for M_2, c) for D_1, d) for D_2.

723

724 Figure 6. Case of M_1 system on March 4-5 2013. a) Time evolution of the fractional areas for
725 different intervals of the CTT value (colored histograms every 15 minutes), minimum CTT (black
726 curve), flash rate (blue curve) and the flash rate density within the area with CTT < -40°C (orange
727 curve). The letters in panel (a) indicate the times for the panels b, c, d and e that show the
728 distribution of the CTT (colored scale) and the location of the flashes (red crosses) detected by

729 WWLLN during 10 minutes around the time of the scan of the cloud by Meteosat radiometer (time
730 indicated in the panels + 6 minutes).
731
732 Figure 7. Same as Figure 6 for M_2 system on March 4-5 2013.
733
734 Figure 8. Same as Figure 6 for D_1 system on December 25, 2013.
735
736 Figure 9. Same as Figure 6 for D_2 storms on December 25, 2013.
737
738 Figure 10. a) Same as Figure 6a for the whole study area over a 44-hour period on December 27-
739 28, 2013. b-d) Lightning flash density at a resolution of 0.1° × 0.1° over the whole study area and
740 for three periods indicated in panel a.
741
742 Figure 11. Temperature of the tropopause calculated at a 2.5° × 2.5° space resolution and averaged
743 for daily values on March 4 (a), December 25 (b), December 27 (c) and December 28 (d). The red
744 frame shows the study area and the small black frames show the storm systems analyzed as
745 indicated in Figure 4a,b.
746
747 Figure 12. Maximum height of the overshoot above the tropopause versus maximum CAPE value
748 for the four case studies analyzed.
749
750
751
752


Height (m)
4000
3000
2000
1500
1000
750
500
250
100
0
ASIA
ATLAS MOUNTAINS
TADEMAIT PLATEAU
Iguidi Desert
Chech Desert
SAHARA
Hoggar
Tahat 2,918 m
Tibesti
Emi Koussi 3,415 m
Libyan Desert
Eastern Desert
Nubian Desert
Red Sea
Air Plateau
SAHEL
Darfur
Gimbala 3,070 m
Ras Dejen 4,533 m
Senegal
Gambia
Niger
Volta
Lake Chad
Nile
Blue Nile
Lake Tana
Fouta Djallon
Loma Mts
Jos Plateau
Adamawa Mts
Adamawa Highland
Mt. Cameroun 4,100 m
ETHIOPIAN HIGHLANDS
Horn of Africa
Somali Peninsula
Cape Hafun
Ogaden Desert
Grain Coast
Ivory Coast
Gold Coast
Slave Coast
Cape Palmas
Gulf of Guinea
Bioko
Principe
São Tomé
Annobón
Cape Lopez
Guinea Basin
EQUATOR
Bornu
Ueki
Congo
Mt. Stanley 5,109 m
Lake Albert
Mt. Elgon 4,321 m
CONGO BASIN
Great Rift Valley
Lake Victoria
Mt. Kenya 5,199 m
Mt. Kilimanjaro 5,895 m
Pemba
Zanzibar
INDIAN OCEAN
Seychelles Islands
Ascension
SOUTH ATLANTIC OCEAN
Angola Basin
KATANGA PLATEAU
BIE PLATEAU
Sena Moco 2,619 m
Lake Tanganyika
Lake Malawi
Rufiji
Mafia
Cape Delgado
Aldabra Islands
Comoros Islands
Cap d'Ambre
Mayotte
St Helena
Cape Fria
Kalahari Desert
Namib Desert
Skeleton Coast
Matopo Hills
Victoria Falls
Lake Kariba
Mozambique Channel
Madagascar
Mauritius
Réunion
Europa
TROPIC OF CAPRICORN
Walvis Ridge
Orange
Vaal
Mont-aux-Sources 3,298 m
Mt. Ntlenyana 3,482 m
Barra Point
Cape Ste. Marie
DRAKENSBERG
Great Escarpment

Figure 1

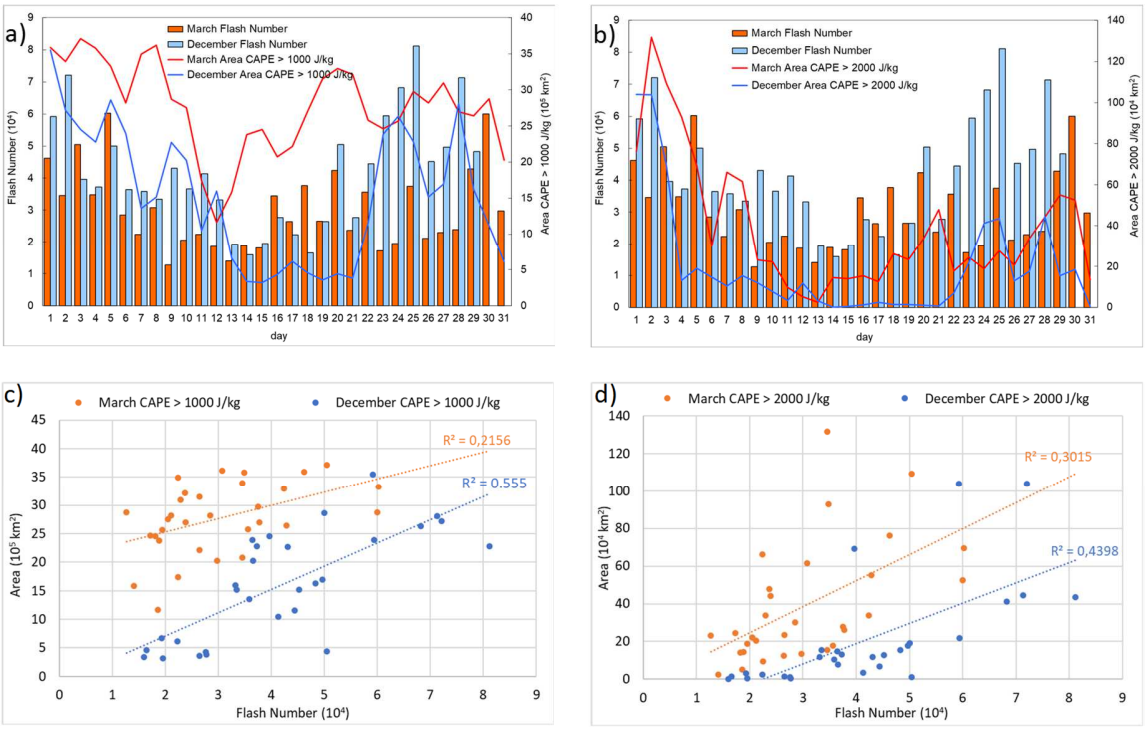
a)
March Flash Number
December Flash Number
March Area CAPE > 1000 J/kg
December Area CAPE > 1000 J/kg
Flash Number (10⁴)
Area CAPE > 1000 J/kg (10⁵ km²)
day
b)
March Flash Number
December Flash Number
March Area CAPE > 2000 J/kg
December Area CAPE > 2000 J/kg
Flash Number (10⁴)
Area CAPE > 2000 J/kg (10⁴ km²)
day
c)
March CAPE > 1000 J/kg
December CAPE > 1000 J/kg
R² = 0,2156
R² = 0.555
Area (10⁵ km²)
Flash Number (10⁴)
d)
March CAPE > 2000 J/kg
December CAPE > 2000 J/kg
R² = 0,3015
R² = 0,4398
Area (10⁴ km²)
Flash Number (10⁴)

Figure 2

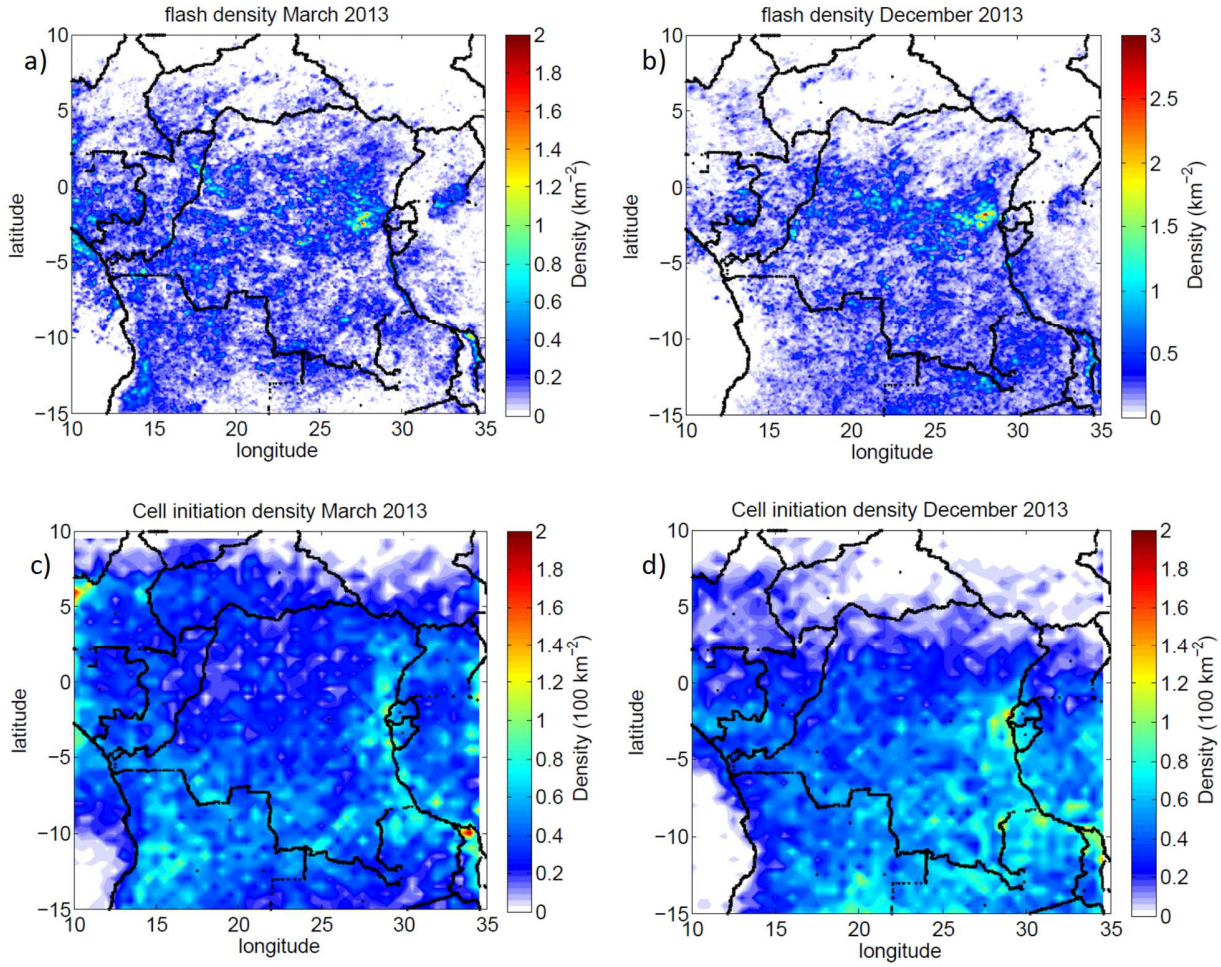
flash density March 2013
a)
flash density December 2013
b)
Cell initiation density March 2013
c)
Cell initiation density December 2013
d)
latitude
longitude
Density (km^{-2})
Density (100 km^{-2})

Figure 3

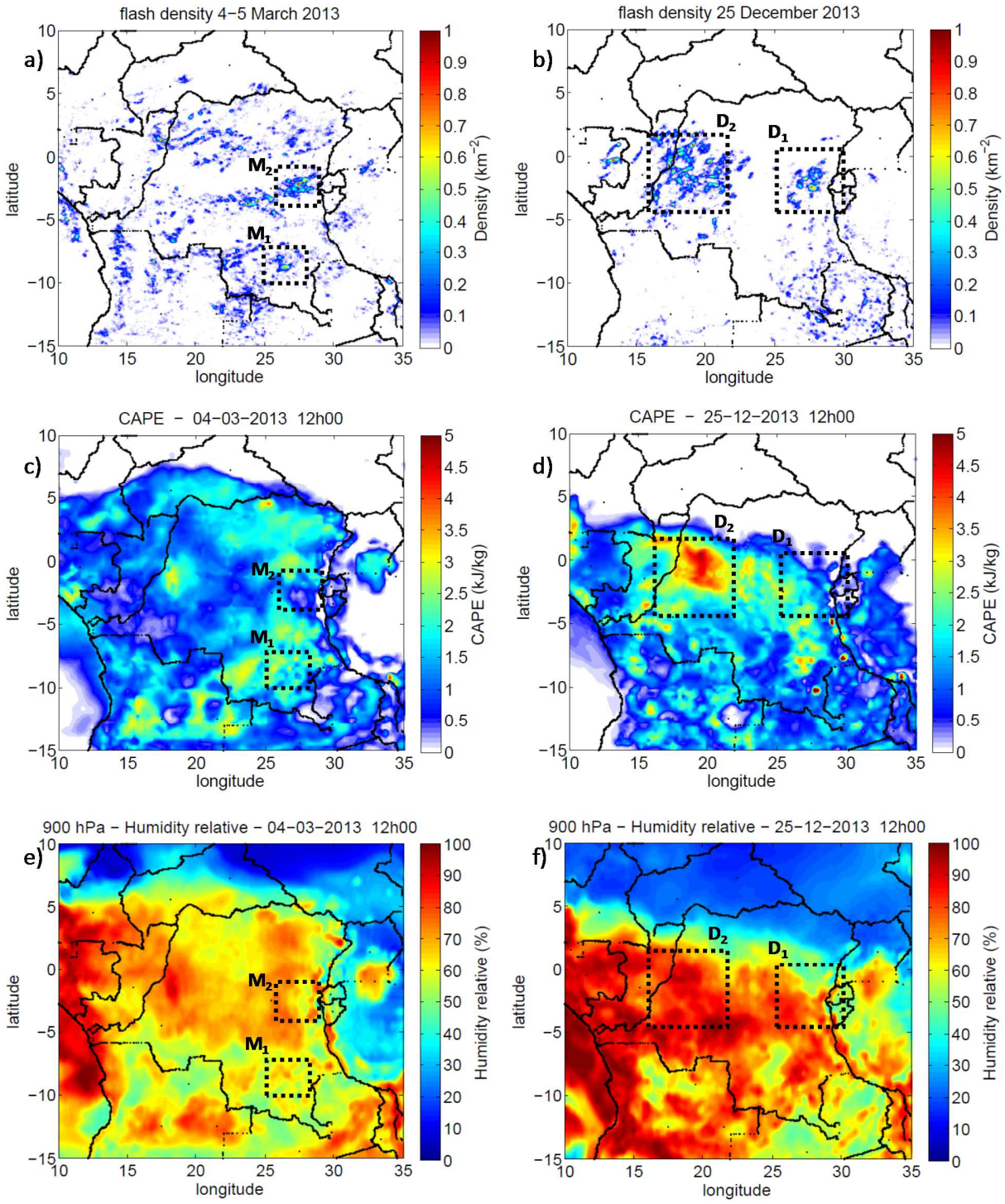
flash density 4−5 March 2013
a)
M2
M1
latitude
longitude
Density (km−2)
flash density 25 December 2013
b)
D2
D1
CAPE − 04−03−2013 12h00
c)
CAPE (kJ/kg)
CAPE − 25−12−2013 12h00
d)
900 hPa − Humidity relative − 04−03−2013 12h00
e)
Humidity relative (%)
900 hPa − Humidity relative − 25−12−2013 12h00
f)

Figure 4

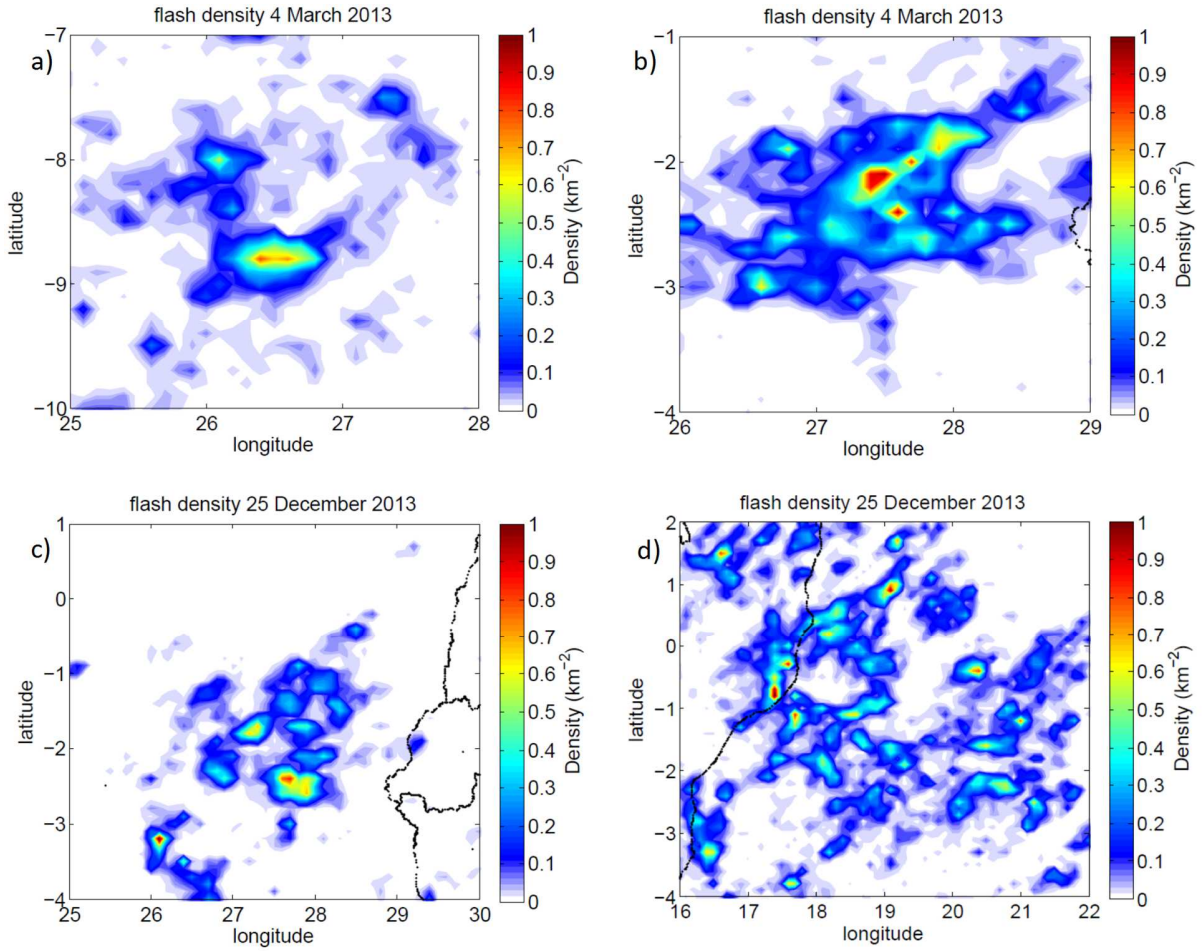
flash density 4 March 2013
a)
b)
flash density 25 December 2013
c)
d)
latitude
longitude
Density (km^{-2})

Figure 5

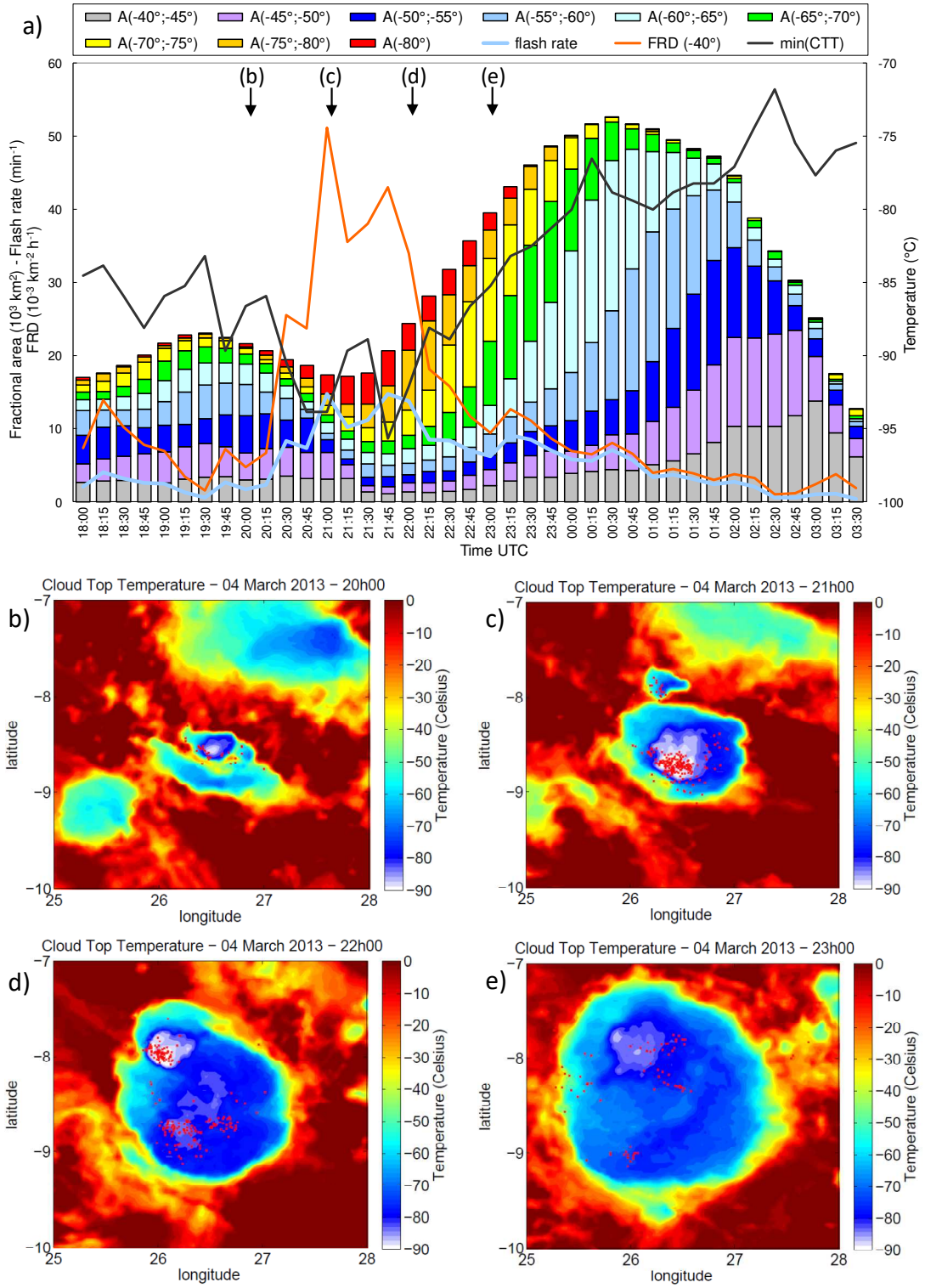
a)
A(-40°;-45°)
A(-45°;-50°)
A(-50°;-55°)
A(-55°;-60°)
A(-60°;-65°)
A(-65°;-70°)
A(-70°;-75°)
A(-75°;-80°)
A(-80°)
flash rate
FRD (-40°)
min(CTT)
(b)
(c)
(d)
(e)
Fractional area (10³ km²) - Flash rate (min⁻¹)
FRD (10⁻³ km⁻² h⁻¹)
Temperature (°C)
Time UTC
b)
Cloud Top Temperature − 04 March 2013 − 20h00
c)
Cloud Top Temperature − 04 March 2013 − 21h00
d)
Cloud Top Temperature − 04 March 2013 − 22h00
e)
Cloud Top Temperature − 04 March 2013 − 23h00
latitude
longitude
Temperature (Celsius)

Figure 6

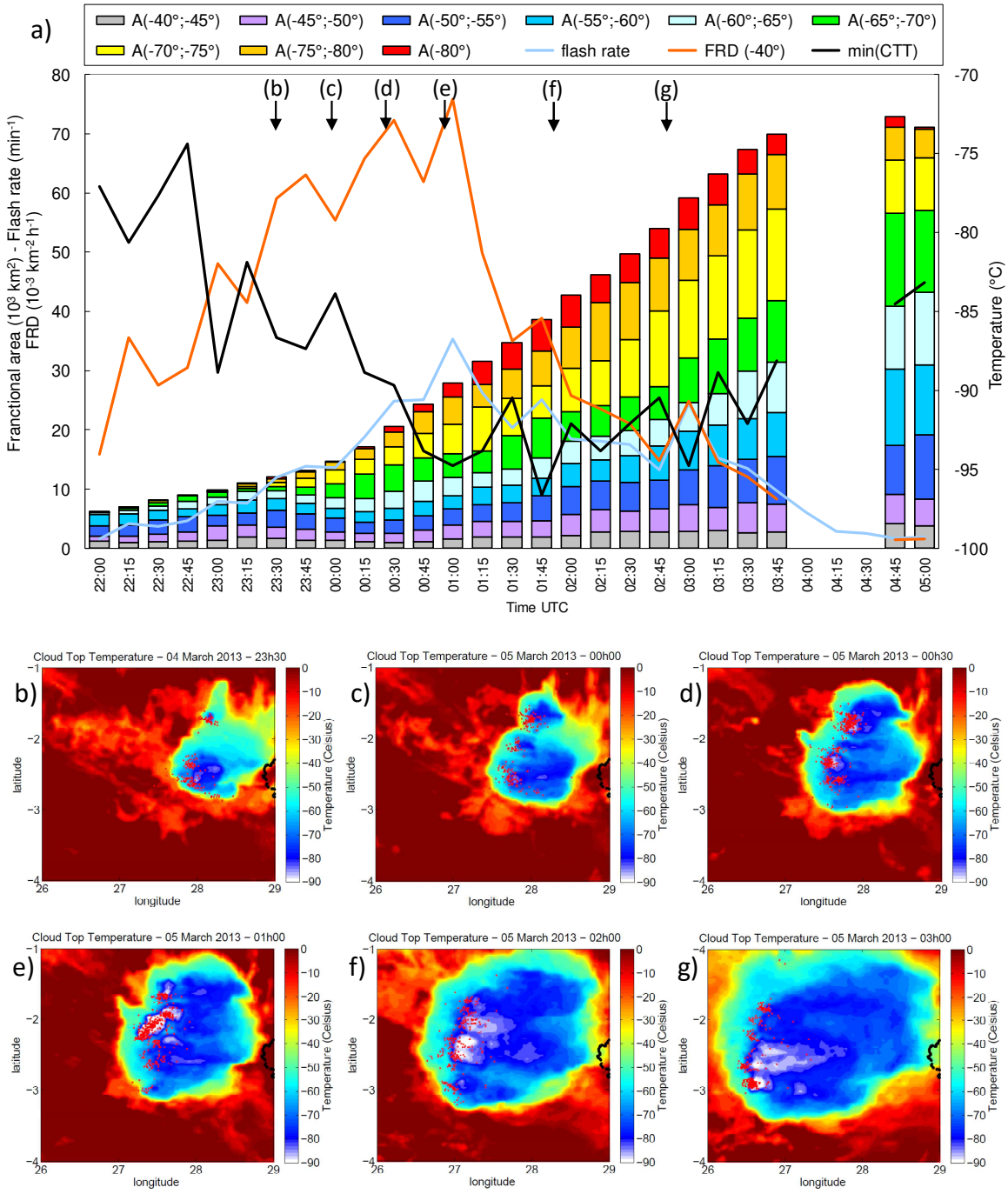
a)
A(-40°;-45°)
A(-45°;-50°)
A(-50°;-55°)
A(-55°;-60°)
A(-60°;-65°)
A(-65°;-70°)
A(-70°;-75°)
A(-75°;-80°)
A(-80°)
flash rate
FRD (-40°)
min(CTT)
(b)
(c)
(d)
(e)
(f)
(g)
Franctional area (10³ km²) - Flash rate (min⁻¹)
FRD (10⁻³ km⁻² h⁻¹)
Temperature (°C)
Time UTC
Cloud Top Temperature – 04 March 2013 – 23h30
Cloud Top Temperature – 05 March 2013 – 00h00
Cloud Top Temperature – 05 March 2013 – 00h30
Cloud Top Temperature – 05 March 2013 – 01h00
Cloud Top Temperature – 05 March 2013 – 02h00
Cloud Top Temperature – 05 March 2013 – 03h00
latitude
longitude
Temperature (Celsius)

Figure 7

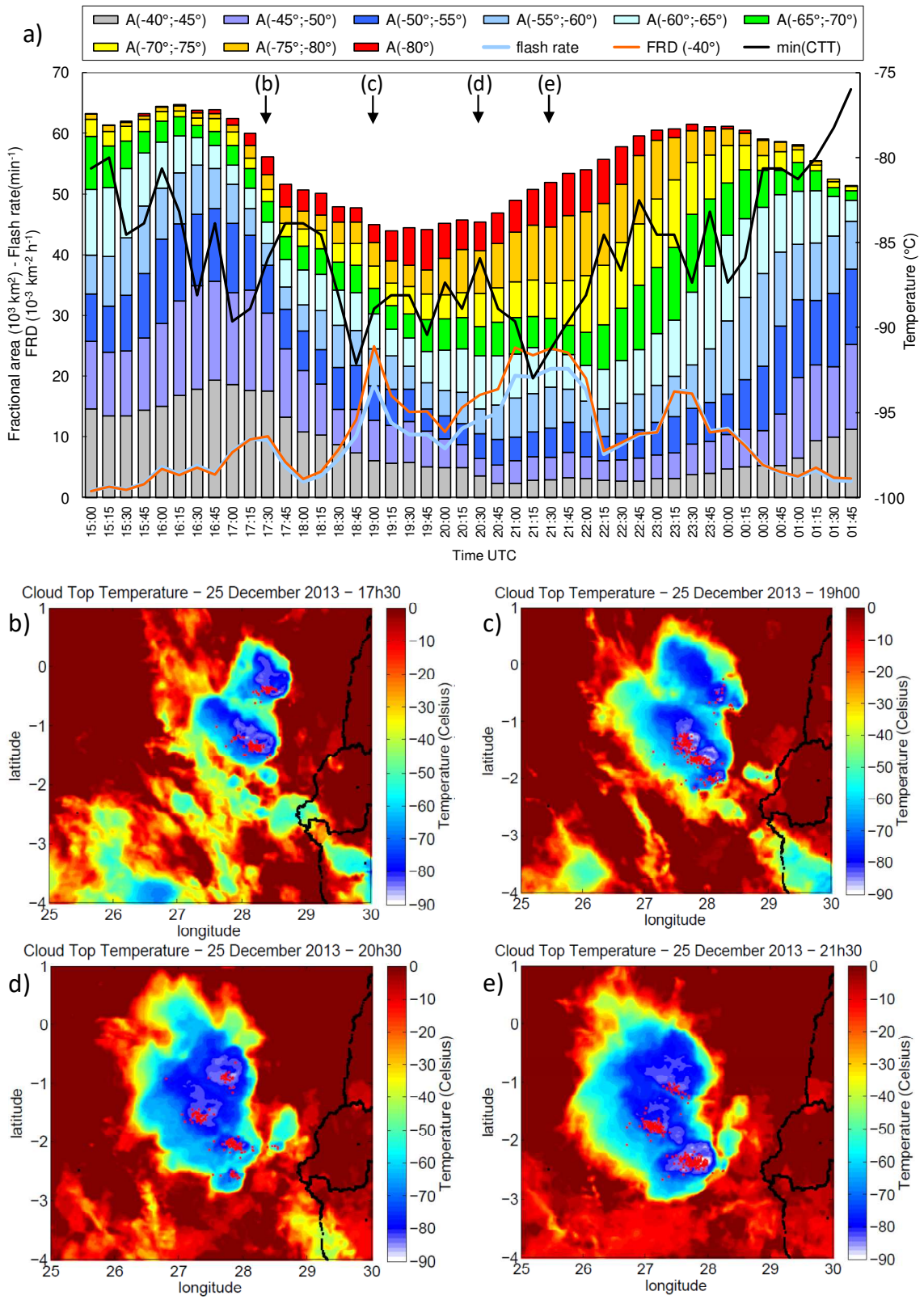
a)
A(-40°;-45°)
A(-45°;-50°)
A(-50°;-55°)
A(-55°;-60°)
A(-60°;-65°)
A(-65°;-70°)
A(-70°;-75°)
A(-75°;-80°)
A(-80°)
flash rate
FRD (-40°)
min(CTT)
(b)
(c)
(d)
(e)
Fractional area (10³ km²) - Flash rate(min⁻¹)
FRD (10⁻³ km⁻² h⁻¹)
Temperature (°C)
Time UTC
b)
Cloud Top Temperature − 25 December 2013 − 17h30
c)
Cloud Top Temperature − 25 December 2013 − 19h00
d)
Cloud Top Temperature − 25 December 2013 − 20h30
e)
Cloud Top Temperature − 25 December 2013 − 21h30
latitude
longitude
Temperature (Celsius)

Figure 8

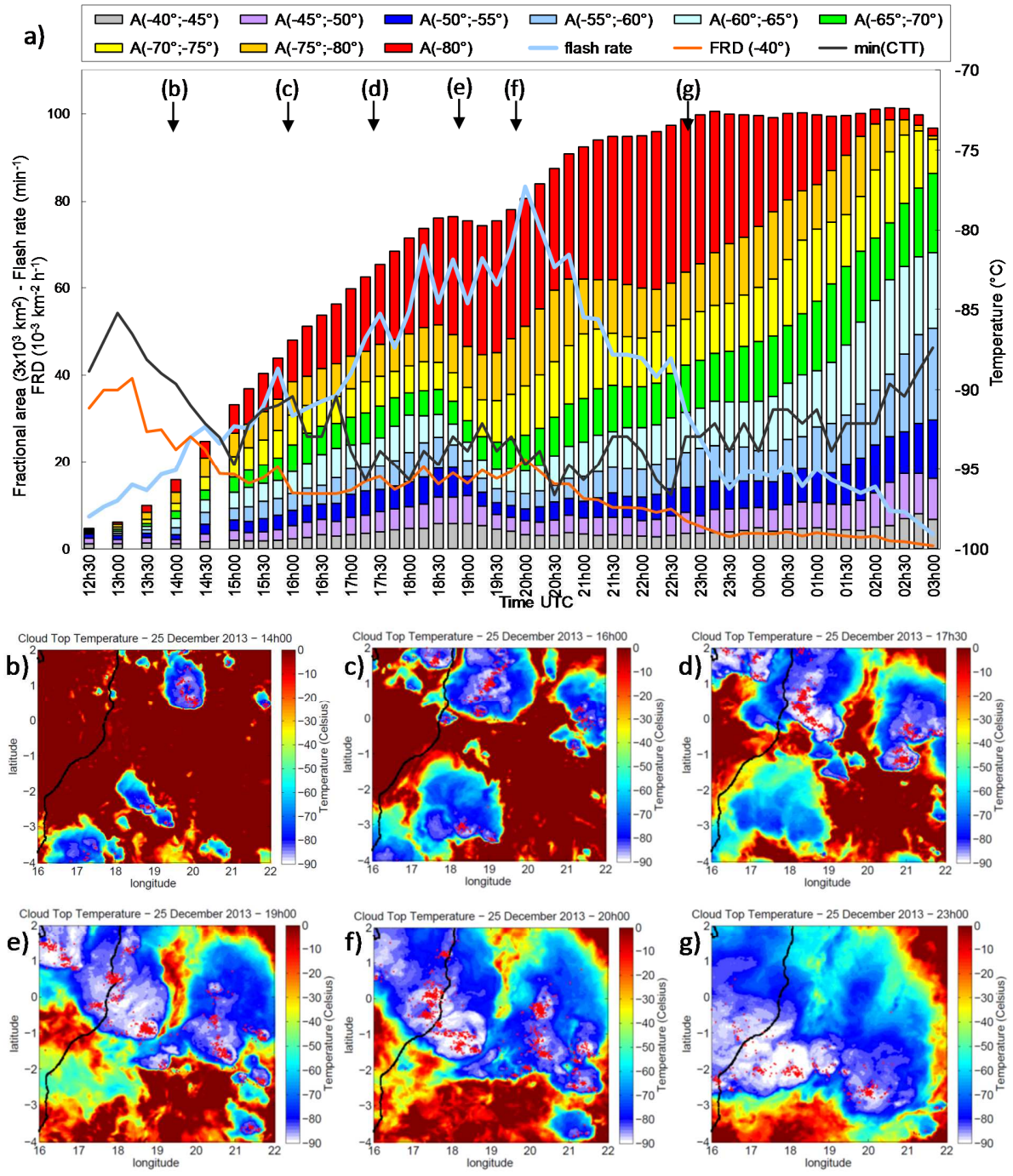
a)
A(-40°;-45°)
A(-45°;-50°)
A(-50°;-55°)
A(-55°;-60°)
A(-60°;-65°)
A(-65°;-70°)
A(-70°;-75°)
A(-75°;-80°)
A(-80°)
flash rate
FRD (-40°)
min(CTT)
(b)
(c)
(d)
(e)
(f)
(g)
Fractional area (3x10³ km²) - Flash rate (min⁻¹)
FRD (10⁻³ km⁻² h⁻¹)
Temperature (°C)
Time UTC
b) Cloud Top Temperature - 25 December 2013 - 14h00
c) Cloud Top Temperature - 25 December 2013 - 16h00
d) Cloud Top Temperature - 25 December 2013 - 17h30
e) Cloud Top Temperature - 25 December 2013 - 19h00
f) Cloud Top Temperature - 25 December 2013 - 20h00
g) Cloud Top Temperature - 25 December 2013 - 23h00
latitude
longitude
Temperature (Celsius)

Figure 9

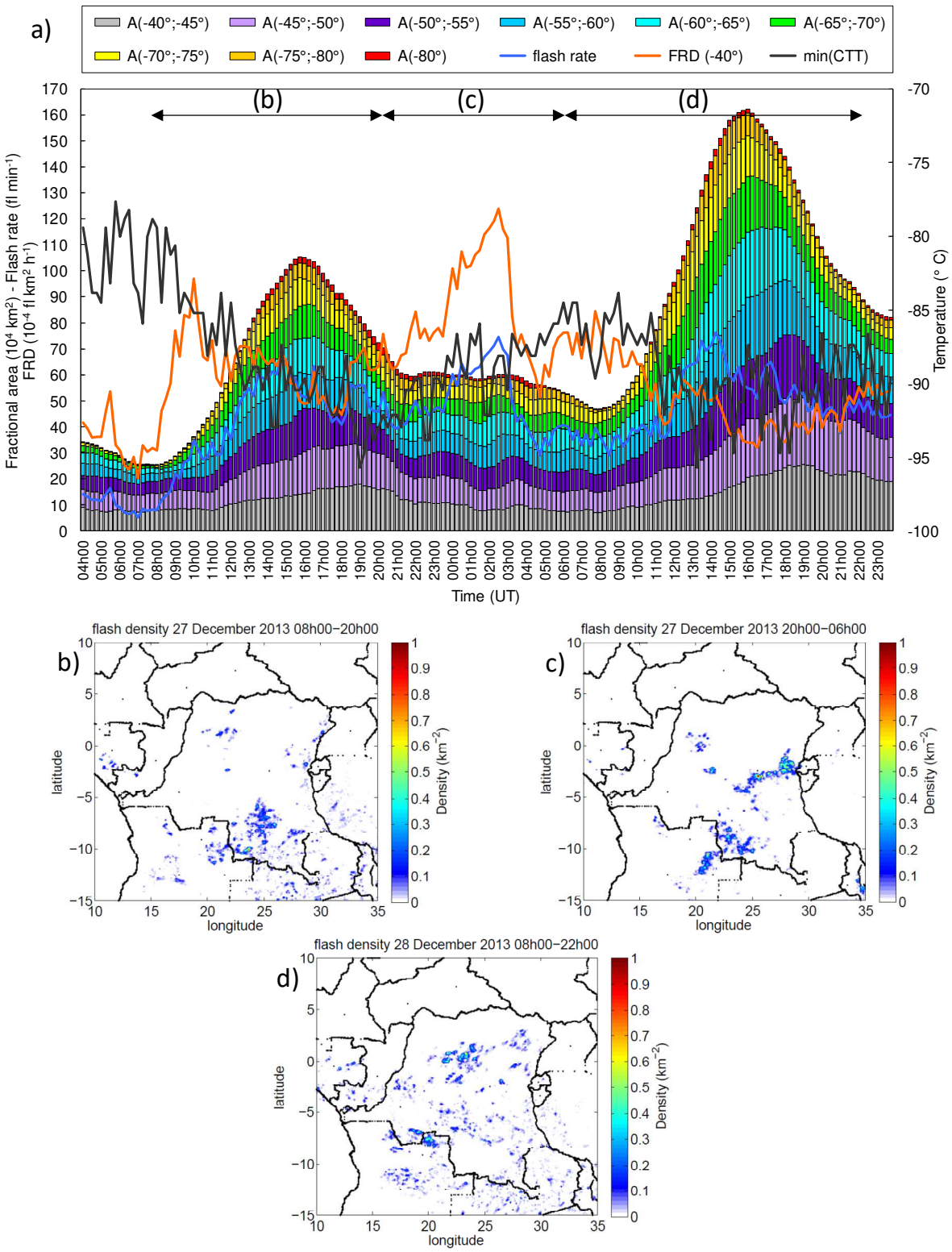

820
821 Figure 10

822

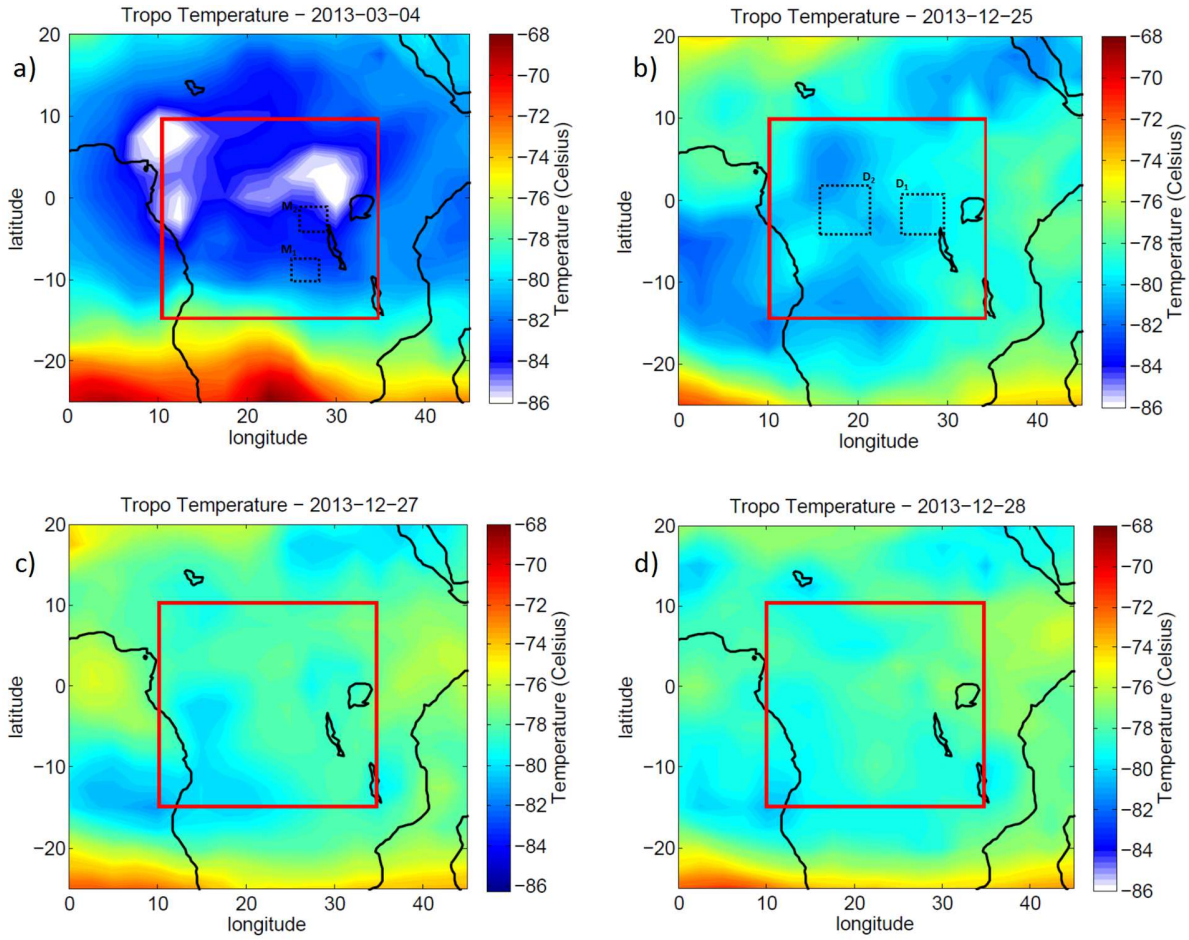
Tropo Temperature – 2013–03–04
a)
Tropo Temperature – 2013–12–25
b)
Tropo Temperature – 2013–12–27
c)
Tropo Temperature – 2013–12–28
d)
latitude
longitude
Temperature (Celsius)
M2
M1
D2
D1

Figure 11

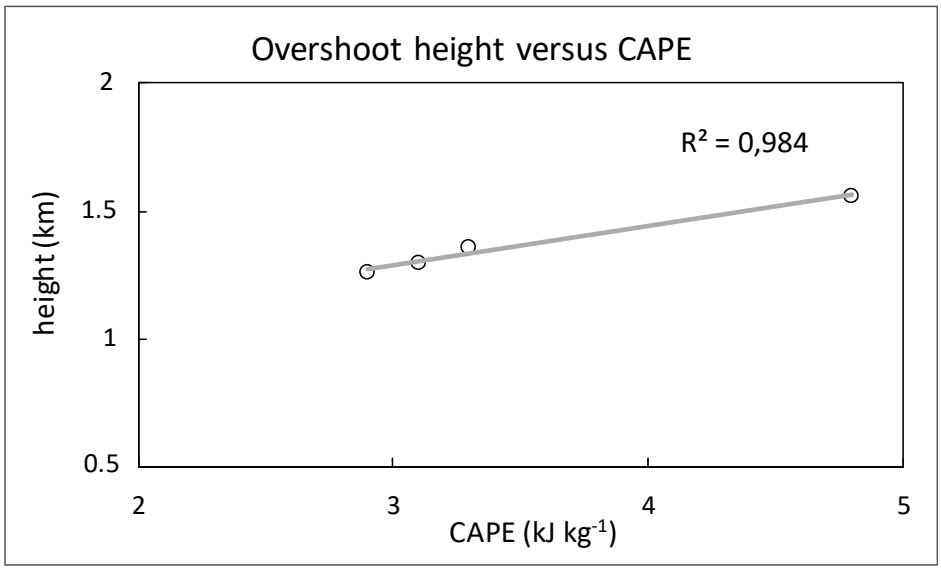

837

838

839 Figure 12.